Performance Tests of a Cryogenic Hybrid Magnetic Bearing for Turbopumps

E. DiRUSSO AND G. V. BROWN

ABSTRACT

Experiments were performed on a Hybrid Magnetic Bearing designed for cryogenic applications such as turbopumps. This bearing is considerably smaller and lighter than conventional magnetic bearings and is more efficient because it utilizes a permanent magnet to provide a bias flux. The tests were performed in a test rig that used liquid nitrogen to simulate cryogenic turbopump temperatures. The bearing was tested at room temperature and at liquid nitrogen temperature (-320 °F). The maximum speed for the test rig was 14 000 rpm.

For a magnetic bearing stiffness of 20 000 lb/in., the flexible rotor had two critical speeds (6300 and 12 600 rpm) within the 14 000-rpm operating range and was operated through both critical speeds. A static (nonrotating) bearing stiffness of 85 000 lb/in. was achieved. Magnetic bearing stiffness, permanent magnet stiffness, actuator gain, and actuator force interaction between two axes were evaluated, and controller/power amplifier characteristics were determined.

The tests revealed that it is feasible to use this bearing in the cryogenic environment and to control the rotordynamics of flexible rotors when passing through bending critical speeds. The tests also revealed that more effort should be placed on enhancing the controller to achieve higher bearing stiffness and on developing displacement sensors that reduce drift caused by temperature and reduce sensor electrical noise.

INTRODUCTION

The cryogenic turbopumps for pumping liquid hydrogen and liquid oxygen to the space shuttle main engines (SSMEs) have experienced serious rotor vibrations. References 1 and 2 describe the hydrogen pump, its associated instabilities, and the effects of seal stiffness and damping on rotor stability. Because of high loading and speed, the rolling element bearings used in the SSME turbopumps have very limited life. Since the bearing compartments of turbopumps contain liquid oxygen or liquid hydrogen, damping schemes typically used in aircraft engines, such as squeeze film dampers, cannot be used. Eddy current dampers [3] or electromagnetic dampers [4] provide limited damping at high frequencies or must be tuned to specific frequency bandwidths. These passive devices cannot be used to actively control rotor stability, and they tend to be large and heavy. It appears that the problems of stability, low damping, and short bearing life can be addressed by using magnetic bearings.

This paper focuses on that application. Since industrial magnetic bearings are typically large and heavy compared with conventional rolling element bearings, a search was made to identify a small, lightweight, and electrically efficient bearing. A hybrid magnetic bearing that utilizes both

---

Eliseo DiRusso and Gerald V. Brown, National Aeronautics and Space Administration, Lewis Research Center, 21000 Brookpark Road, MS 23-3, Cleveland, Ohio 44135.

permanent magnets and electromagnets was chosen. This bearing was designed for cryogenic application by Avcon, Inc., and NASA Lewis Research Center. The Avcon bearing is discussed in References 5, 6, and 7. This hybrid concept differs from others in that the permanent magnets are arranged such that the electromagnet flux does not pass through them, which results in higher efficiency.

Other efficient hybrid magnetic bearings have been designed. References 8 and 9 describe a permanent magnet biased magnetic bearing that integrates a thrust bearing along with the radial bearing. This bearing was designed for room temperature application. The testing demonstrated that the use of permanent magnets can improve operating efficiency over conventional, all-electromagnet designs.

To linearize the force-to-current relationship for magnetic bearings, one must provide a "bias flux." The current industrial practice is to supply the bias flux with electromagnets, which means that electrical power is required full time to supply the bias flux. In the hybrid bearing, the permanent magnet supplies the bias flux without power expenditure, resulting in a large power saving. Reference 5 compares bearing size, weight and power consumption of the hybrid and conventional magnetic bearings. The weight and size of the power amplifier electronics are also significantly reduced for the hybrid bearing in comparison to all-electromagnet bearings.

The hybrid bearing built for this study is 5.25 in. in diameter, 4.5 in. long, and weighs 17.4 lb. Its bore is 3.03 in., and its air gap is 0.024 in. The radial load capacity is 500 lb (linear load limit is approximately 320 lb at room temperature) and could be substantially increased by optimization.

The objectives of this research were to

(1) Determine the feasibility of using magnetic bearings in cryogenic turbopumps

(2) Apply magnetic bearings to control the rotordynamics of supercritical rotors such as those found in the SSME turbopumps

(3) Explore any special problems in applying magnetic bearings to turbopumps

TEST RIG AND MAGNETIC BEARING

TEST RIG

The test rig simulates a rotor and the cold environment of a cryogenic turbopump. This rig, originally designed to evaluate eddy current and electromagnetic dampers, was modified to incorporate the hybrid bearing and to operate at cryogenic conditions. The rig has a unique capability of applying measured forces to the shaft to measure magnetic bearing stiffness and permanent magnet forces at both room temperature and liquid nitrogen temperature. A drawing of the rig is shown in Figure 1. The rotor has a vertical axis and is supported by the magnetic bearing at the bottom and a preloaded duplex ball bearing at the top. The magnetic bearing carries only radial load, and the ball bearing carries radial and thrust load. The rotor is driven by an ac motor through a belt and pulley speed increaser (2 to 1 ratio) at speeds up to 14 000 rpm. The rotor has a primarily rigid body and a bending critical speed within the operating range, and it can be unbalanced by placing set screws in one of the disks. For cryogenic operation, liquid nitrogen at -320 °F submerges the magnetic bearing, and liquid level is controlled by a sensing system. A vacuum chamber (Figure 1) reduces the liquid boil-off rate.

MAGNETIC BEARING

The key magnetic bearing components can be seen in Figure 1. These are the ferromagnetic rotor, rotor laminations, stator laminations, stator windings, samarium cobalt permanent magnet, pole piece, and position sensors. The backup bearing shown at the bottom of the shaft positions the rotor when the magnetic bearing is not operating. When the rotor is centered, there is a 0.010-in. radial gap between the rotor and the backup bearing.

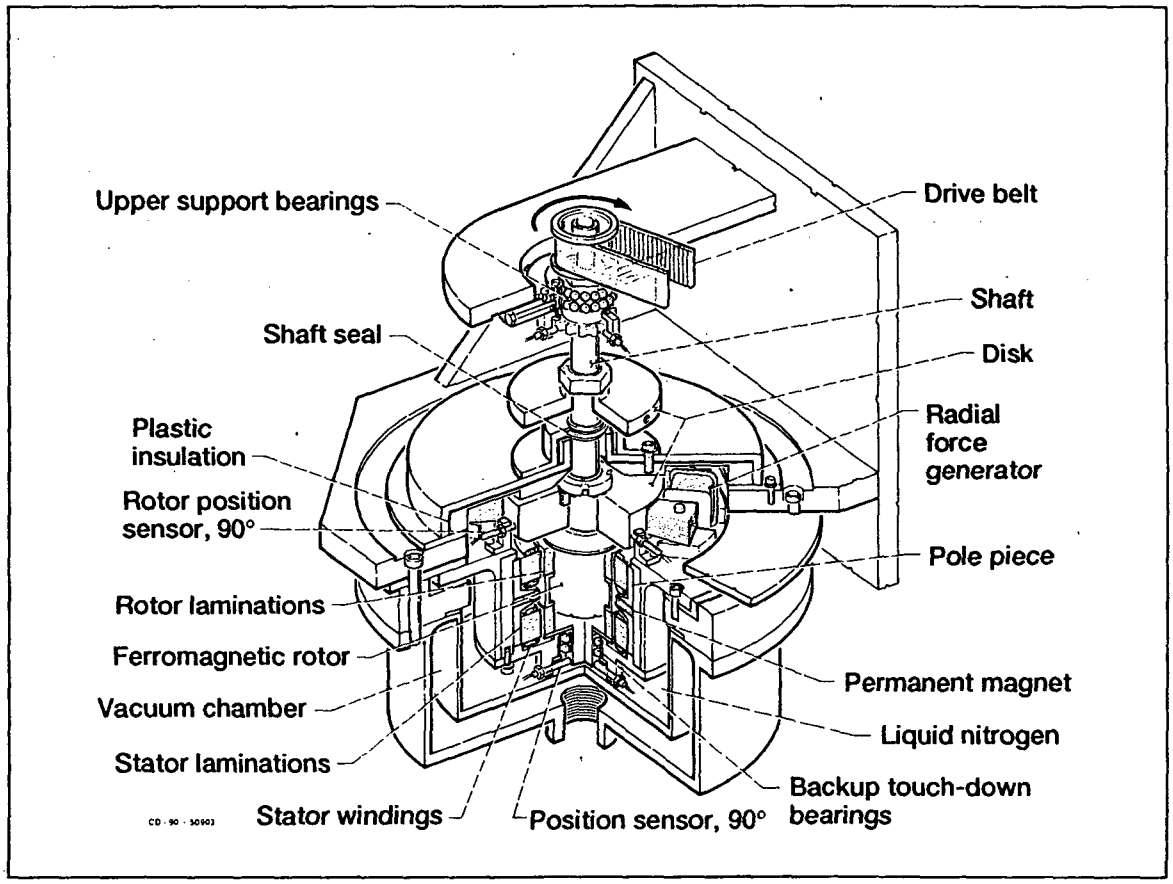

Figure 1.—Cryogenic hybrid magnetic bearing and test rig.

DISPLACEMENT SENSORS

Eight eddy current position sensors were used to control the bearing (Figure 1). Four probes located below the magnetic bearing measured orthogonal displacements at the end of the shaft. For each axis (X and Y), the difference between the signals from two diametrically opposed probes was used as the position signal. This reduced the effect of shaft surface irregularity on the control signal and reduced the zero shift in the probe signals between room temperature and liquid nitrogen temperature. The same was done for the four probes located above the bearing. Since the upper and lower probes were equidistant from the bearing center, a simple average of the upper and lower probe signals provided control signals that were, in effect, co-located with the axial center of the magnetic bearing. Stable levitation was not possible with only the upper set of probes. Stable levitation was possible with only the lower set at low stiffness.

CONTROLS

All results presented in this paper were obtained with a simple proportional derivative or proportional integral derivative analog controller. The schematic of the control circuit for one bearing axis is shown in Figure 2. The component values shown produced a measured stiffness of 20 to 22 lb/mil. The summer at the front end of the circuit added the signals from the displacement sensors that were above and below the bearing to obtain a value proportional to the displacement at the bearing center. The measured transfer function of the controller is shown in Figure 3. The derivative was limited to a 1.5-kHz bandwidth, and the overall control was limited to a 3-kHz bandwidth by the low pass filter.

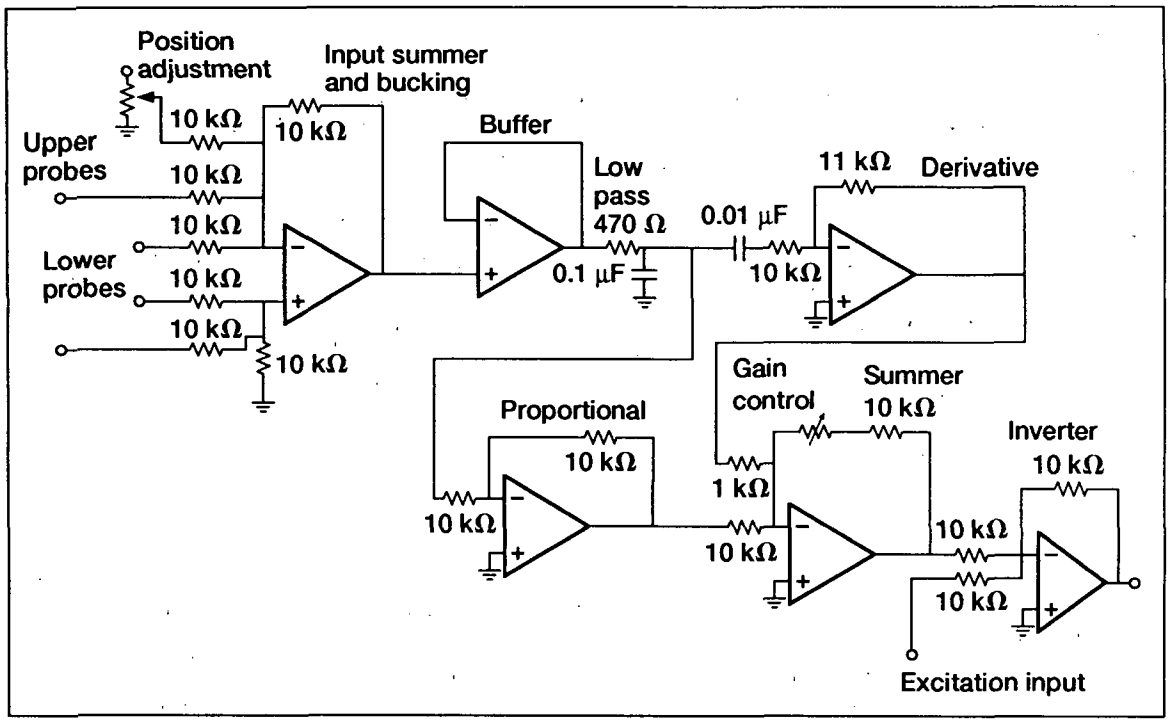

Figure 2.—Analog control system for hybrid magnetic bearing.

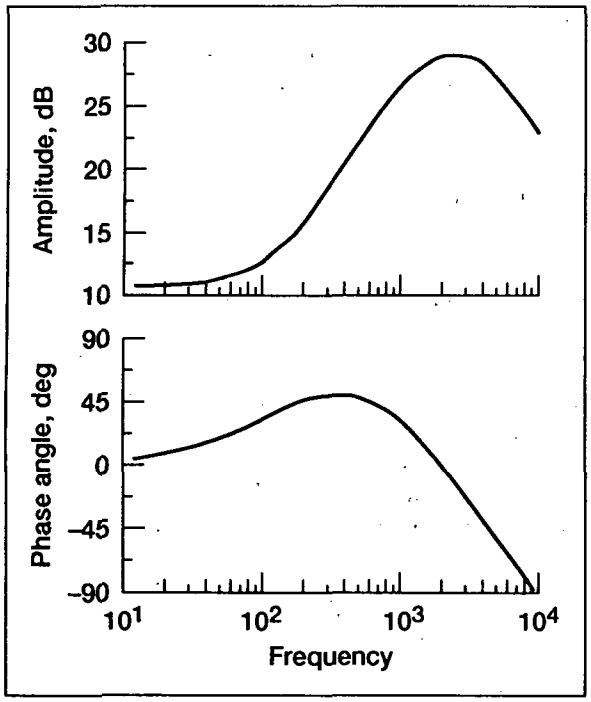

Figure 3.—Transfer function for analog controller.

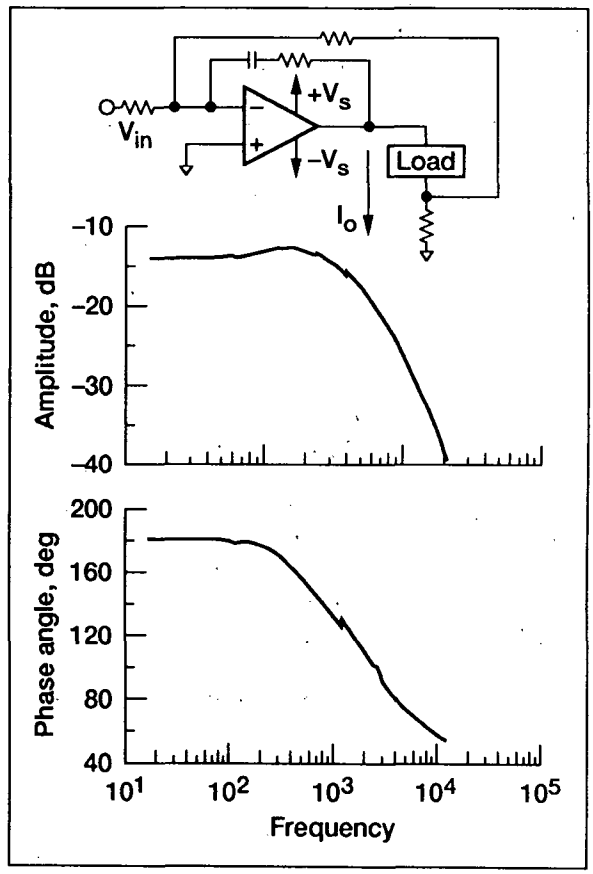

Figure 4.—Transfer function for power amplifiers.

POWER AMPLIFIERS

Linear transconductance power amplifiers were used for the laboratory tests, even though weight and size limitations would probably require switching amplifiers for potential flight versions. The circuit diagram for the amplifiers is shown in the inset of Figure 4. The resistive-capacitive feedback circuit, required for stability, limits the bandwidth of the amplifier to about 1.5 kHz, as shown by the amplifier transfer function between input voltage V_{in} and output current I_o in Figure 4. This somewhat marginal bandwidth is a consequence of the 1-MHz gain-bandwidth product of the hybrid power operational amplifier used and the 35-mH inductance being driven. An increase in bandwidth of a factor of 2 to 4 would be preferred. The maximum voltage output of the amplifier is about 65 V, and steady currents of 10 A or more are well within its safe operating area.

ACTUATOR PERFORMANCE

PERMANENT MAGNET STIFFNESS

The position stiffness due to the permanent magnet alone is an important design parameter for this type of bearing. It was measured by positioning the rotor on the backup bearing (magnetic bearing power off) and applying a force at the bottom of the shaft (just below the lower position sensors) while simultaneously measuring the applied force and shaft radial position at the center of the magnetic bearing. As the force was applied, the shaft moved smoothly and continuously toward the radial center of the bearing. The permanent magnet force at the axial center of the magnetic bearing was calculated from the measured force by taking moments about the top bearing giving $F_{pm} = 1.27F_{me}$, where F_{pm} is the permanent magnet force at the axial center of the magnetic bearing, and F_{me} is the measured force at the bottom of the shaft.

The permanent magnet force versus displacement is shown in Figure 5. The experimental value of stiffness, derived from a linear curve fit through the force versus displacement data, was -19 000 lb/in. at room temperature. Permanent magnet stiffness measurements made at liquid nitrogen temperature varied between -13 000 and -21 000 lb/in. Since this measurement was made before the differential probe system was installed, temperature changes caused considerable drift in the displacement data at liquid nitrogen temperature, causing scatter in the stiffness measurement. The permanent magnet stiffness is expected to increase at liquid nitrogen temperature.

ACTUATOR GAIN

Figure 6 shows experimental data for the electromagnet force versus current for room temperature and liquid nitrogen temperature. The actuator gain is the slope of this curve and, for the linear portion, is 89 lb/A for both room temperature and liquid nitrogen temperature. The linear portion extends out to approximately 320 lb for room temperature and approximately 350 lb for liquid nitrogen temperature with some unexplained assymmetry with respect to positive and negative current. The actuator gain as a function of rotor radial position was found to be independent of radial position within approximately 5 percent. Data for these curves were acquired by stabilizing the shaft at the bottom and measuring the radial force reaction at the bottom end of the shaft with load cells as current was applied to the actuator coils. The force at the axial center of the magnetic bearing was calculated from the measured reaction at the bottom of the shaft by taking moments about the top bearing:

$$F_{mb} = 1.27R_{me} \tag{1}$$

where F_{mb} is the total force exerted by the magnetic bearing at its axial center (sum of electromagnet and permanent magnet forces), and R_{me} is the measured reaction at the bottom of the shaft.

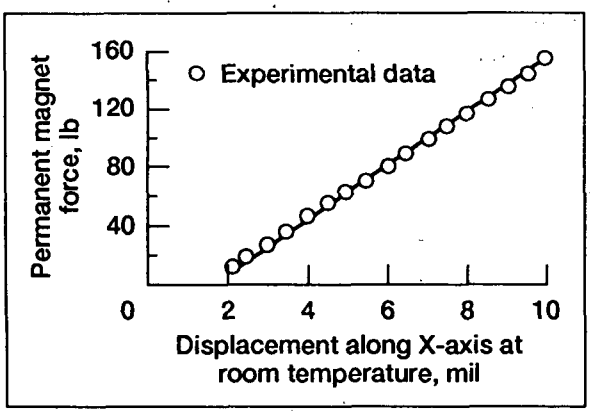

Figure 5.—Permanent magnet force as function of rotor radial position.

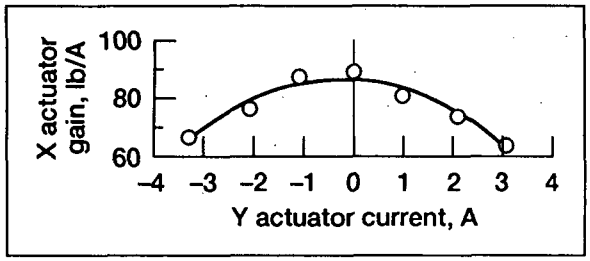

Figure 7.—X actuator gain as function of Y current at room temperature.

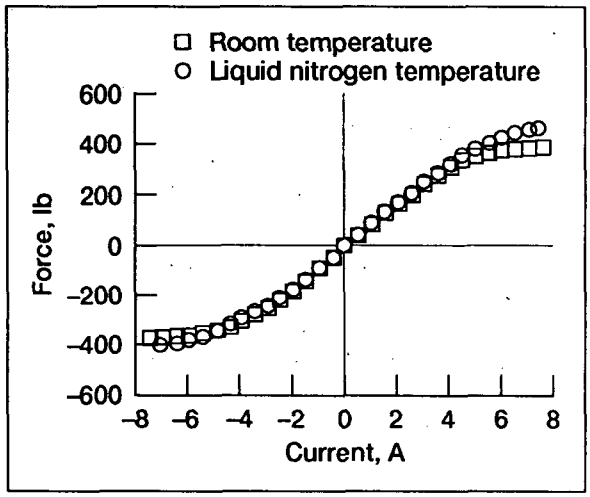

Figure 6.—Electromagnetic force as function of current.

A correction was required because of shaft deflection as the actuator force was applied. This deflection caused the permanent magnet to pull on the shaft in the same direction as the actuator force. Therefore, the reaction measured by the load cells was due to the sum of the electromagnet force and the permanent magnet force. The permanent magnet force was calculated by multiplying the measured permanent magnet stiffness (described above) by the measured shaft deflection, hence

$$F_{em} = F_{mb} - k_{pm}(s) \tag{2}$$

where F_{em} is the electromagnet force, F_{mb} is the total force exerted by the magnetic bearing, K_{pm} is the permanent magnet stiffness, and s is the shaft deflection at the axial center of the bearing.

X/Y FORCE INTERACTION

During the testing of the bearing, a force interaction between the X and Y axes was noticed. This interaction was evaluated by measuring the X actuator gain as the Y actuator current was varied. The results are shown in Figure 7. The figure shows that, for zero current in the Y actuator, the X actuator gain is approximately 89 lb/A, and at 3 A of Y actuator current, the X actuator gain falls off to approximately 65 lb/A. The reason for this is not yet understood. This degree of interaction between the two axes can cause control and stability problems.

MAGNETIC BEARING STIFFNESS

The magnetic bearing stiffness was obtained by levitating the shaft and applying a known force at the bottom of the shaft while simultaneously measuring the displacement at the center of the

magnetic bearing. The force exerted by the magnetic bearing was calculated using the known force by taking moments about the top bearing center line. The magnetic bearing stiffness (Δ force/Δ displacement) was calculated from these data. Static (nonrotating) stiffness from 10 000 lb/in. up to 85 000 lb/in. was achieved while preserving stability. The highest stiffness achieved for the rotating tests was approximately 46 000 lb/in. The stability of the bearing as the stiffness is increased needs further work.

ROTOR PERFORMANCE

ROTOR CRITICAL SPEEDS AND MODE SHAPES

The first two rotor critical speeds are strongly dependent on the magnetic bearing stiffness. Figure 8 shows the analytically determined mode shapes for the first two modes for a magnetic bearing stiffness of 15 300 lb/in. and a top bearing stiffness of 800 000 lb/in. The first mode, occurring at 5460 rpm, is primarily a rigid body mode but has some shaft bending in it because of the high degree of shaft flexibility. The second mode, occurring at 12 200 rpm, has the character of a first bending mode. These are typical mode shapes for the first two modes for magnetic bearing stiffnesses below about 30 000 lb/in. When the magnetic bearing stiffness is increased to about 45 000 lb/in., the first mode becomes first bending in character. This is illustrated in Figure 9, which shows the first mode for a magnetic bearing stiffness of 46 500 lb/in. Figure 10 is an analytically determined plot of critical speed versus magnetic bearing stiffness for the first two modes.

ROTATING TESTS

Rotating tests were performed for magnetic bearing stiffnesses from 10 000 lb/in. to 22 000 lb/in. at room temperature and liquid nitrogen temperature and at 46 000 lb/in. at room temperature. The rotor was finely balanced for these tests (i.e., no intentional unbalance was applied). For a magnetic bearing stiffness of approximately 20 000 lb/in., the bearing was operated up to 14 000 rpm, which is the full speed capability of the rig.

Figures 11(a) and (b) show the orbits at the lower and upper measuring planes for room temperature. Figure 11(c) shows the voltage applied to the actuator coils (Y voltage plotted against X voltage) for a magnetic bearing stiffness of 20 000 lb/in. and a speed of 14 000 rpm. This type of plot clearly reveals whether the power amplifier voltage limits (rails) are reached. Exceeding this voltage limit causes nonlinear behavior. The nearly square shape of the voltage "orbits" may be due to the axis interaction effect mentioned above. The orbits and voltages for liquid nitrogen operation were similar to those at room temperature but with somewhat larger orbit amplitude.

For this stiffness, the first critical speed was traversed at 6300 rpm, and the second critical speed was traversed at 12 600 rpm (see Rotor Critical Speeds and Mode Shapes). The amount of damping offered by the controller was such that amplitude peaks at these speeds were not markedly evident in the orbit traces. These frequencies were observed, however, in the spectral map shown in Figure 12. The plot shows a resonance at 105 Hz (6300 rpm), which is the first critical speed, and another resonance at 210 Hz (12 600 rpm), which is the second critical. Note that the amplitudes of the critical speeds in the spectral map were very small indicating a large amount of damping. The half-order and higher order harmonics are evidence of nonlinearities. The half-order harmonic is evident in the orbits, which require two revolutions before repeating.

Rotating tests were also performed at a bearing stiffness of approximately 46 000 lb/in. at room temperature. The orbits for displacement were similar to those for the 20 000-lb/in. stiffness. The bearing was operated up to 10 000 rpm through the bending mode, which occurred at approximately 7600 rpm. Amplitude buildup at the first critical speed was not observed for this case either. At 10 000 rpm, an instability was encountered at this stiffness. Higher power amplifier voltage and improved compensation that were made to the controller after these tests were performed should permit operation to 14 000 rpm at this stiffness.

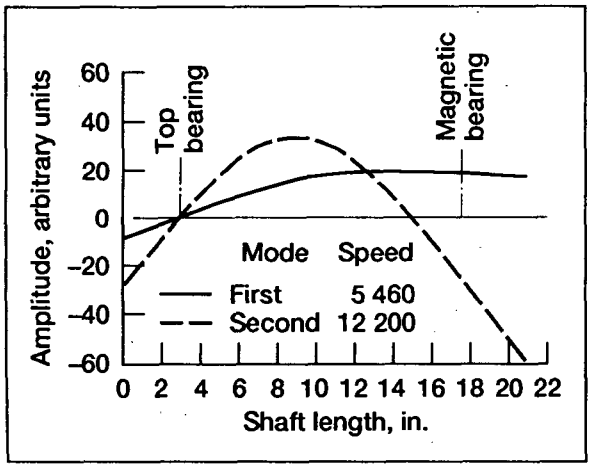

Figure 8.—Shaft mode shapes for magnetic bearing stiffness of 15 300 lb/in. (analytical data). Top bearing stiffness, 800 000 lb/in.

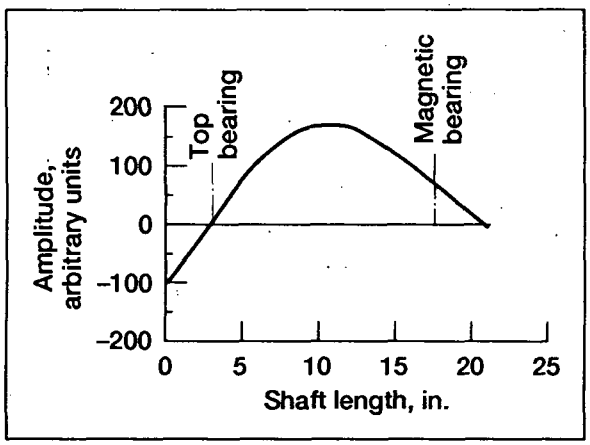

Figure 9.—Shaft first mode shape for magnetic bearing stiffness of 46 500 lb/in. (analytical data). Top bearing stiffness, 800 000 lb/in.

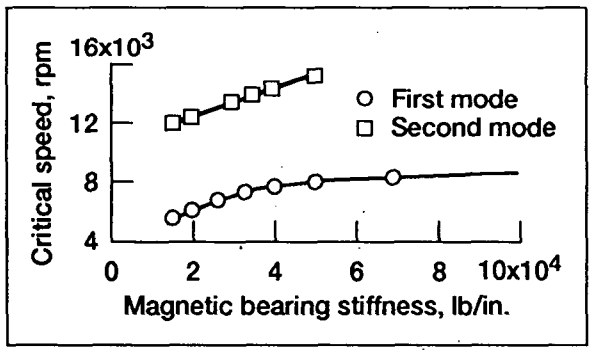

Figure 10.—Shaft critical speed as function of magnetic bearing stiffness (analytical data). Top bearing stiffness, 800 000 lb/in.

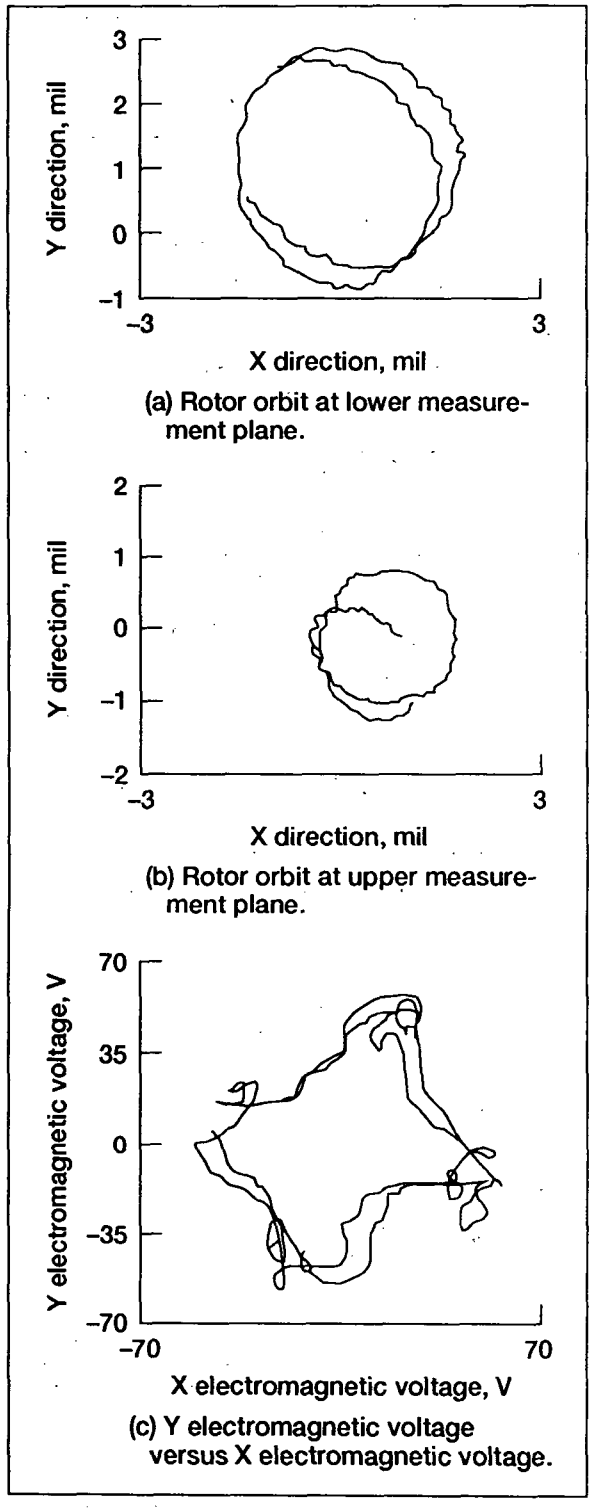

Figure 11.—Rotor orbits and electromagnet voltage. Speed, 14 000 rpm; magnetic bearing stiffness, 20 000 lb/in.; room temperature.

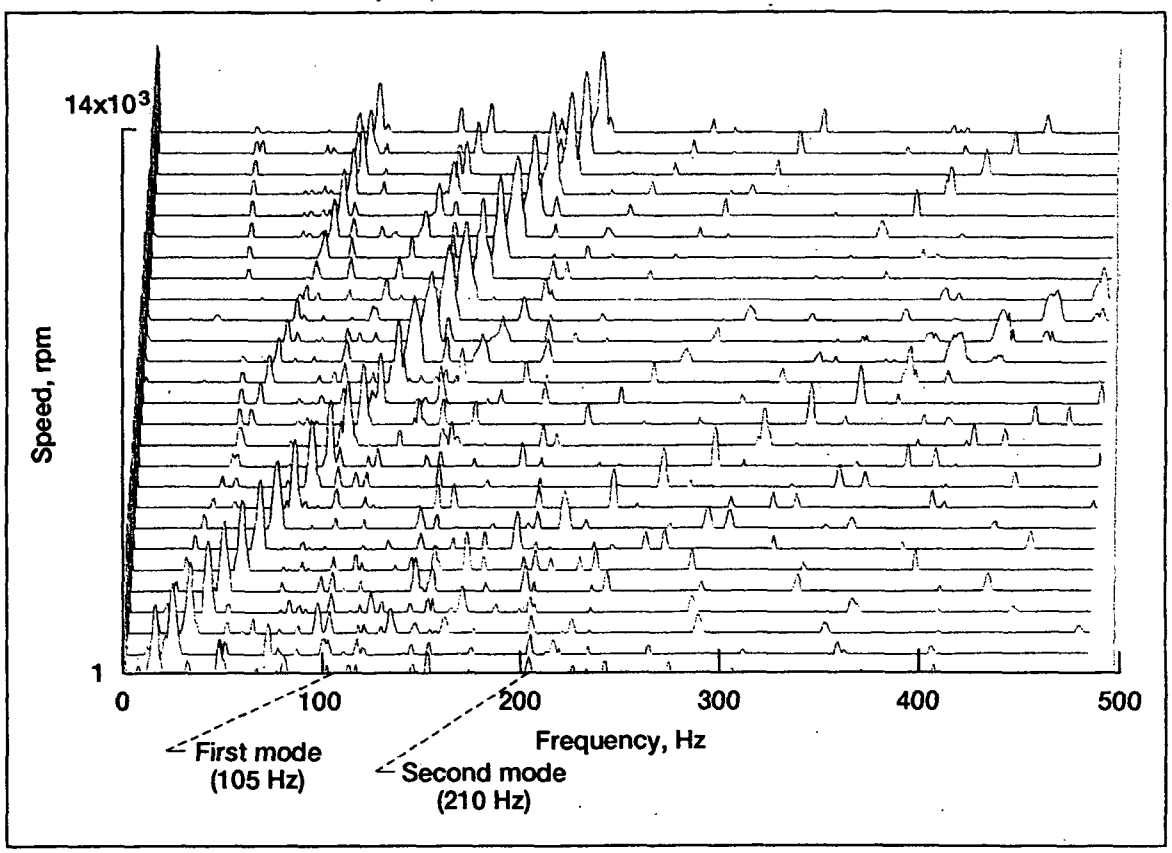

Figure 12.—Spectral map for room temperature operation. Magnetic bearing stiffness, 20 000 lb/in.

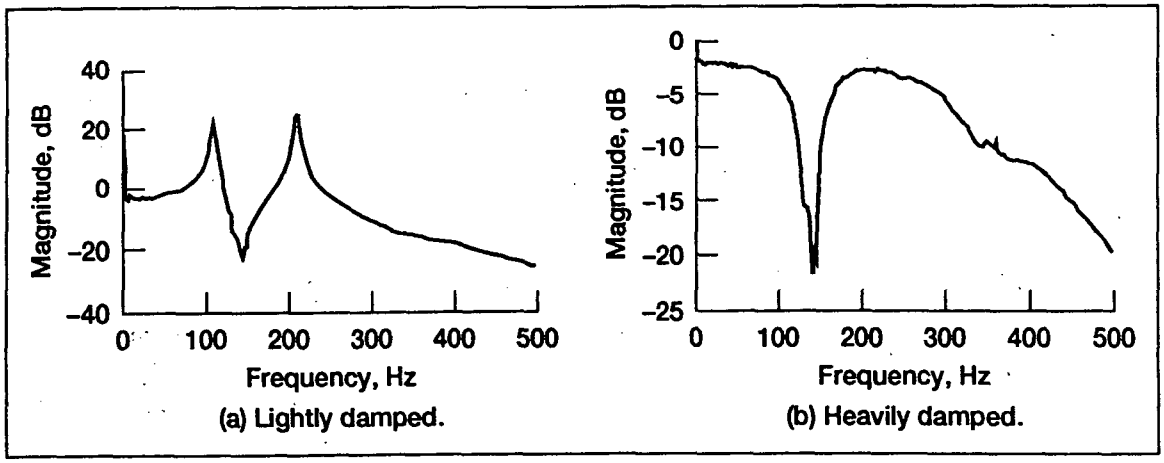

Figure 13.—Transfer function between noise into magnetic bearing controller and lower displacement probes. Magnetic bearing stiffness, 20 000 lb/in.

The damping provided by the controller was reduced to verify the frequency of the two critical speeds. The bearing was levitated (nonrotating), and the rotor was excited by noise fed into the controller. A transfer function between noise into the bearing and the upper and lower displacement probes was taken. Figures 13(a) and (b) show the transfer function at the lower displacement probes for light and heavy damping, respectively, and clearly indicate that the two modes are present when the damping is reduced.

UNIQUE BEARING CHARACTERISTICS

This bearing, like those described in References 8 and 9, differs from early hybrid designs by avoiding placement of the electromagnets (EM's) and the permanent magnets (PM's) in a disadvantageous, simply-connected series magnetic circuit. One must be careful, however, about considering the EM and PM fluxes to be independent. In this bearing one might like to say that the permanent magnet flux lies in a plane parallel to the axis and the control flux in a plane perpendicular to the axis. This viewpoint is helpful, and we can apply the magnetic circuit approximation independently to the PM flux and to the EM flux, only as long as the magnetic material responds linearly (so that superposition is valid) wherever the two fields coexist. If the magnetic material becomes nonlinear where the fields coexist, this simplification is not permissible.

A viewpoint valid even in saturation is to consider the total field strength (rather than its vector components) at each point in space. In this view, when the EM is off, the permanent magnet flux divides equally between the stator poles at each end of the bearing, producing four north poles at one end and four south poles at the other. To apply maximum load, the electromagnets double the strength of one pole at each end of the bearing and reduce the strength of the opposing poles to zero. The other poles are unchanged. The field at the PM remains essentially unchanged, but the field lines bend circumferentially as they approach the stators and pass through the back iron. (A similar shift must occur in the rotor and journals.) Field lines that, at zero current, would pass through the pole that is nullified at maximum current, pass through the neighboring poles, and half of the flux from those poles moves around to the double-strength pole. This viewpoint of tracing total field lines is valid even in saturation, a regime into which aerospace demands of high load capacity and light weight may push the design.

An advantage of the homopolar geometry is that the field excursions experienced by the rotor are reduced in frequency and magnitude, reducing rotor heating by magnetic hysteresis and by eddy currents. In an eight-pole radial bearing with a pole order of NSNSNSNS, the rotor experiences four hysteresis loops per revolution under no load. For a pole order of NSSNNSSN, there are two loops per revolution, interleaved with two smaller loops in which the field does not change sign (because of the gaps between stator poles). At maximum load toward one EM, the rotor sees poles NSNS00NS (underscoring means double strength) in the first case and NSSN00SN in the second. Therefore, there are one double-size loop and two "regular" loops per revolution in the first case and one double loop, one half loop, and one regular loop in the second. In the homopolar design, there are four half loops under no load, and at maximum load (toward a pole) there are one double-size half loop and two half loops. Thus, the potential for rotor heating by either of the two mechanisms is much lower.

As noted above, the flux through the PM is independent of the control currents if the iron is below saturation. Hence the two ends of the bearing can be operated as independent actuators if separate power amplifiers are used. Increasing the number of actuation points along the rotor axis increases the degree of controllability. The problem of a flexible mode with a node at the bearing axial center is virtually eliminated, since only very high frequency modes could have nodes near both ends of the bearing; one end or the other will have some mode shape upon which to act.

An equivalent way of viewing the capability of two independent actuators is to say that the bearing can exert moments as well as forces on the shaft. This would work best in the otherwise worst-case situation discussed above (a node at the center of the bearing), because the slope of the mode shape is greatest there. As long as both actuators remain in the linear operating range, forces and moments are available simultaneously (at the price of twice as many power amplifiers).

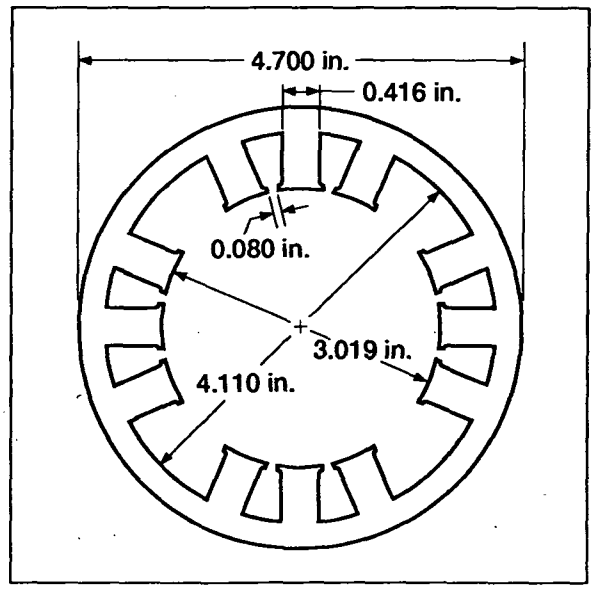

Figure 14.—Stator laminations.

POTENTIAL FOR HIGHER PERFORMANCE

A very substantial increase in load capacity should be possible in a growth version of this bearing without much change in the bearing physical envelope. To save time and cost during construction, the stator laminations were stamped by existing dies for electric motor laminations, with one pole per quadrant removed for the bearing, as shown in Figure 14. The ratio of pole leg cross-sectional area to pole face area at the gap is 0.81, so the gap field strength is limited to that fraction of the field strength in the legs. A custom stamping would increase the flux capacity of each quadrant by about 30 percent and the load capacity by over 55 percent before allowing for worse leakage and fringing. More ampere turns per unit of flux would be needed, but the coils presently operate far from any thermal limit even at room temperature. Moderate changes in cross section of other parts of the flux paths might be required to support the increased flux. The radial air gap, presently 0.024 in., could be decreased by 20 percent or more to reduce the gap reluctance and allow the permanent magnet to provide the higher bias field without an increase in size.

CONCLUDING REMARKS

These tests have shown that it is feasible to use the hybrid magnetic bearing in the cryogenic environment and to control the rotordynamics of flexible shafts when operating at or above the bending critical speeds. The bearing and test rig have met their original objectives in terms of load capacity, operating speed, and performance at critical speeds. Somewhat higher performance at liquid nitrogen temperature had been expected from the samarium-cobalt permanent magnet, permitting linear force versus current behavior to 500-lb load capacity. This needs further exploration.

The bearing behaves as a reasonably linear actuator. The negative spring due to the permanent magnet is close to linear, and the actuator gain (current stiffness) is approximately independent of shaft position and load to around 320 lb. The presence of half-order excitations in the frequency analysis of rotating data, however, indicates some degree of nonlinearity somewhere in the system. The interaction of forces between bearing axes needs to be explained.

Although this hybrid magnetic bearing is much smaller and lighter than commercial magnetic bearings, for turbopump applications the size and weight should be reduced further. This can be achieved through optimization of the present design. Also the control system must be developed to

improve the stability margin at higher bearing stiffness (upwards of 100 000 lb/in). The "moment control" capability of this bearing should help to achieve the higher stiffness.

The position sensors are problematic when used in the cryogenic environment because of position signal drift due to temperature change. The differential probe system was instituted to mitigate this problem, but more work needs to be done regarding sensor sensitivity to temperature change. Also electrical noise inherent in the sensors strongly affects stability for high values of stiffness and damping, so this aspect must be explored.

REFERENCES

1. Ek, M.C., 1980. "Solving Subsynchronous Whirl in the High-Pressure Hydrogen Turbomachinery of the SSME." Journal of Spacecraft, 17(3):208-218.

2. Ek, M.C., July 1978. "Solution of the Subsynchronous Whirl Problem in the High Pressure Hydrogen Turbomachinery of the Space Shuttle Main Engine." AIAA Paper 78-1002.

3. Cunningham, R.E., Feb. 1986. "Passive Eddy-Current Damping as a Means of Control in Cryogenic Turbomachinery." NASA TP-2562.

4. DiRusso, E., and G.V. Brown, 1990. "Experimental Evaluation of a Tuned Electromagnetic Damper for Vibration Control of Cryogenic Turbopump Rotors." NASA TP-3005.

5. Meeks, C.R., et al., 1990. "Design of a Highly Efficient Magnetic Bearing For Cryogenic Applications," in Advanced Earth-to-Orbit Propulsion Technology, R.J. Richmond and S.T. Wu, eds. NASA CP-3092-VOL-2, pp. 442-445.

6. Meeks, C.R., E. DiRusso, and G.V. Brown, 1990. "Development of a Compact, Light Weight Magnetic Bearing." AIAA/SAE/ASME/ ASEE 26TH Joint Propulsion Conference, July 16-18, 1990, Orlando, Florida.

7. Avcon Inc., Dec. 1991. Cryogenic Magnetic Bearing Test Facility (CMBTF), NASA CR-189087.

8. Sortore, C.K., et al., 1990. "Permanent Magnet Biased Magnetic Bearings—Design, Construction and Testing." 2nd International Symposium on Magnetic Bearings, July 12-14, 1990, Tokyo, Japan.

9. Sortore, C., et al., 1990. "Design of Permanent Magnet Biased Magnetic Bearings for a Flexible Rotor, Mechanical Failures Prevention Meeting, April 1990, Virginia Beach, Virginia.